Nanomechanical displacement detection using coherent transport in ordered and disordered graphene nanoribbon resonators

A. Isacsson[*]

Department of Applied Physics, Chalmers University of Technology, SE-412 96 Göteborg Sweden.
[*]*Corresponding author: andreas.isacsson@chalmers.se*

(Dated: Version: October 5, 2010)

Graphene nanoribbons provide an opportunity to integrate phase-coherent transport phenomena with nanoelectromechanical systems (NEMS). Due to the strain induced by a deflection in a graphene nanoribbon resonator, coherent electron transport and mechanical deformations couple. As the electrons in graphene have a Fermi wavelength $\lambda_F \sim a_0 \approx 1.4$ Å, this coupling can be used for sensitive displacement detection in both armchair and zigzag graphene nanoribbon NEMS. Here it is shown that for ordered as well as disordered ribbon systems of length L, a strain $\epsilon \sim (w/L)^2$ due to a deflection w leads to a relative change in conductance $\delta G/G \sim (w^2/a_0 L)$.

Nanoelectromechanical (NEM) resonators hold promise for technological implementations such as tunable RF-filters and ultrasensitive mass-sensing. NEMS are also of interest in connection with fundamental studies of quantum properties of macroscopic systems. Regardless of application area, transduction mechanisms for system control and readout must be implemented.

Being only a single atomic layer thick, graphene constitutes the ultimate material for 2D-NEMS, and graphene NEMS have already been demonstrated [1–6]. Because electron transport through mesoscopic graphene devices can be phase coherent [7–9], using graphene in NEMS means that phase coherent transport phenomena can be directly integrated into NEM resonators. This allows the motion of the NEMS to couple to the length scale set by the Fermi wave length $\lambda_F \sim a_0 \approx 1.4$ Å.

So far graphene NEMS have operated in the diffusive transport regime where electric [5, 6] transduction has been based on charge carrier density modulation. In those experiments the graphene was suspended above a backgate a distance d as shown in Fig. 1(a). For a sheet of length L and width W the capacitance to the gate is $C_G \approx \epsilon_0 L W/d$ [10, 11]. Hence, the backgate voltage V_G induces a carrier density $n_0 e = \epsilon_0 V_G/d$. This leads to a conductivity of $\sigma = \mu \epsilon_0 V_G/d$ [12], where μ is the mobility. Motion detection then uses the change in carrier density with distance. For a deflection w away from the equilibrium distance d, the relative change in conductance is $\delta\sigma/\sigma \sim w/d$ [13]. Note that only geometric length scales (w and d) enter into this expression.

A deflection w also induces strain $\epsilon \approx (w/L)^2$, which affects both the dynamical [5, 14] and the electronic [15] properties. For diffusive transport, strain leads to a linear increase in resistance [16] with a constant of proportionality of order unity. Hence, the relative change in conductivity due to strain, $\delta\sigma_{\mathrm{strain}}/\sigma \sim (w/L)^2$, is typically negligible compared to that from the carrier density modulation (for a more detailed anaysis, see Ref. [13]).

The situation is different if one considers coherent transport in graphene nanoribbons. The transverse confinement then give rise to conductance quantization.
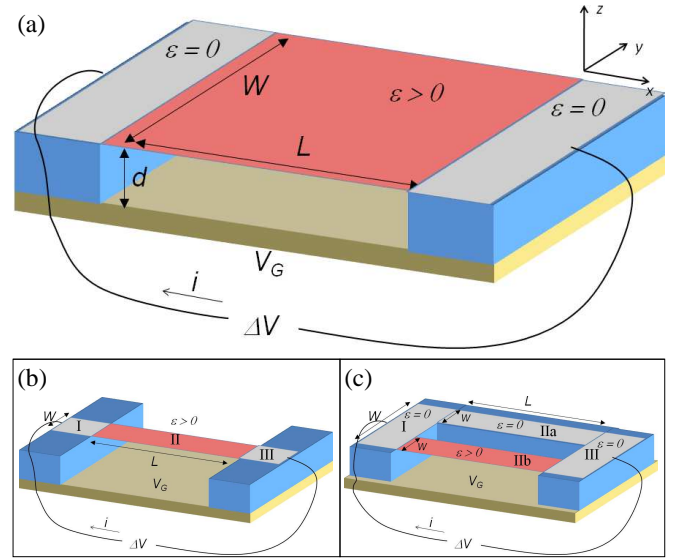

FIG. 1: (Color online) Suspended graphene NEMS systems. (a) Graphene sheet of length L and width W suspended in the $xy-$plane above a backgate. (b) Single suspended nanoribbon. For armchair nanoribbons, the strain induces a transport gap which can be used for displacement detection. (c) Graphene nanoribbon interferometer for displacement detection using zigzag nanoribbons.

This prevents conductance changes due to motion in the backgate electrostatic field leaving strain as the only coupling between deformation and conductance. In this paper it is shown that in such graphene nanoribbon NEM-devices, an operating point where σ changes with displacement as $\delta\sigma/\sigma = \delta\sigma_{strain}/\sigma \sim (w^2/a_0 L)$ can be found. For armchair nanoribbons [see fig. 1(b)], this is due to the opening of the transport gap. For zig-zag nanoribbons, which has no transport gap, an interferometer type set-up [see Fig. 1(c)] can be used. This set-up can also be used in the presence of edge-disorder.

Typically, graphene NEMS in equilibrium is not under zero strain. Not only will this inhibit ripple formation, it will also lead to more linear mechanical response. This

strain can either be due built in strain or due to biasing to a working point w_0. In the latter case, the sensitivity to a variation $w = w_0 + \delta w$ in deflection is naturally linear in δw, i.e. $\delta G/G \sim (w^2/a_o L) \approx (w_0/L)(\delta w/a_0)$.

Transport through suspended graphene sheets and ribbons and in graphene with strained regions has been studied previously by several researchers [17–20] and the prospects of using strain in a controlled way to influence electronic properties is currently an active research field. Here the focus is on displacement detection in graphene nanoribbon NEMS.

The electronic properties close to the charge neutrality point are well described by the nearest neighbor tight binding model. Suppressing spin indices it is

$$H = -\sum_{n,\delta_i} \left[t_{n\delta_i} a_n^\dagger b_{n\delta_i} + \text{h.c.} \right] + \sum_m [V_m^{(a)} n_m^{(a)} + V_m^{(b)} n_{m\delta_1}^{(b)}]. \tag{1}$$

Here $a_n^\dagger$ is the creation operator for an electron at the point $\mathbf{R}_n = (n_1 \mathbf{a}_1 + n_2 \mathbf{a}_2)$ and $b_{n\delta_i}$ the destruction operator for electrons at the site $\mathbf{R}_n + \delta_i$. The basis is here: $\mathbf{a}_1 = a_0(3/2, \sqrt{3}/2)$, $\mathbf{a}_2 = a_0(3/2, -\sqrt{3}/2)$, $\delta_1 = a_0(1/2, \sqrt{3}/2)$, $\delta_2 = a_0(1/2, -\sqrt{3}/2)$, and $\delta_3 = a_0(-1, 0)$. For unstrained graphene, $t_{n\delta} = t_0 \approx 2.7$ eV, and the Fermi velocity is $\hbar v_F = 3t_0 a_0/2$.

For uniform strain ϵ along the $x-$direction (armchair edge) the bond-lengths change from a_0 to

$$|\delta_1| = |\delta_2| = a_0[1 + 0.25\epsilon(1 - 3\sigma_p)], \quad |\delta_3| = a_0[1 + \epsilon],$$

while for uniform strain in the y-direction (zig-zag edge),

$$|\delta_1| = |\delta_2| = a_0[1 + 0.25\epsilon(3 - \sigma_p)], \quad |\delta_3| = a_0[1 - \epsilon\sigma_p].$$

Here $\sigma_p \approx 0.1$ is the Poisson ratio.

The changed lengths alter the hopping energies as $t_{n\delta_i} = t_0(1 + \Delta_i)$. Typically, $\epsilon \ll 1$ and it suffices to work to first order in ϵ. As $\Delta_i \propto \epsilon$, only first order terms in Δ_i need to be kept. The spectrum then remains gapless and linear and can, for uniform strain, be described by the low energy Hamiltonian $H = H_D + V$ where

$$H_D = \hbar v_F \begin{bmatrix} \hat{\Sigma} \cdot (-i\nabla + \mathbf{k}_0) & 0 \\ 0 & \hat{\Sigma}^* \cdot (-i\nabla - \mathbf{k}_0) \end{bmatrix}.$$

Here $\hat{\Sigma}$ is a modified $\hat{\sigma}$-matrix defined as

$$\hat{\Sigma} \equiv v_F^{-1} \begin{bmatrix} 0 & \mathbf{v} \\ \mathbf{v}^* & 0 \end{bmatrix} = v_F^{-1} \begin{bmatrix} 0 & v_x\hat{x} + v_y\hat{y} \\ v_x^*\hat{x} + v_y^*\hat{y} & 0 \end{bmatrix} \tag{2}$$

where

$$\hbar v_x = \frac{3t_0 a_0}{2} \left[1 + \frac{\Delta_1 + \Delta_2 + 4\Delta_3}{6} - i\frac{\sqrt{3}}{3}\frac{\Delta_1 - \Delta_2}{2} \right]$$

$$\hbar v_y = \frac{3t_0 a_0}{2} \left[\frac{\Delta_1 - \Delta_2}{2\sqrt{3}} - i\left(1 + \frac{\Delta_1 + \Delta_2}{2}\right) \right]$$

$$\mathbf{k}_0 = \frac{1}{3a_0} \left(\sqrt{3}[\Delta_2 - \Delta_1], \; \Delta_1 + \Delta_2 - 2\Delta_3 \right).$$

Hence, the Fermi velocity changes and becomes anisotropic, and the locations of the Fermi points in wavevector space changes.

The Δ_i:s depend on the direction the strain is applied in and must be determined from first principles. In the context of carbon nanotubes, this has been studied extensively [21–23] mainly using tightbinding Hückel theory or Koster-Slater calculations [24]. More recently, density functional theory has been applied to strained graphene [25, 26]. Here, the model of Ribeiro et al. [26] will be used, where $t_{\delta_i} = t_0 \exp[-\beta_i(\delta_i/a_0 - 1)]$.

For strain along the $x-$direction (armchair) $\beta_1 = \beta_2 = 2.6$, $\beta_3 = 3.3$ [26], and to lowest order in ϵ, one finds

$$\hat{\Sigma} = (1 - 2.35\epsilon)\sigma_x\hat{x} + (1 - 0.46\epsilon)\sigma_y\hat{y}, \tag{3}$$

$$\mathbf{k}_0 = \frac{2}{3a_0}2.84\epsilon\hat{y}. \qquad (armchair) \, (4)$$

Here $\sigma_{x,y}$ are the conventional Pauli spin-1/2 matrices. For strain along the $y-$direction (zig-zag) $\beta_1 = \beta_2 = 3.15$ and $\beta_3 = 4$ [26], which gives

$$\hat{\Sigma} = (1 - 0.74\epsilon)\sigma_x\hat{x} + (1 - 2.30\epsilon)\sigma_y\hat{y}, \tag{5}$$

$$\mathbf{k}_0 = -\frac{2}{3a_0}2.70\epsilon\hat{y}. \qquad (zig-zag) \, (6)$$

Consider now an armchair graphene nanoribbon of length L, uniform width W, suspended above a backgate as in Fig. 1(b). The supported parts (regions I and III) are assumed to be unstrained, while the suspended part (region II) is under finite strain $\epsilon > 0$. The conductance in the linear response regime is related to the transmission function $\mathcal{T}(E)$ as $G = 2(e/h^2)\mathcal{T}(E)$, where the prefactor 2 accounts for spin.

Confinement in the y-direction leads to quantization of transverse wavevector components $q_n = 2\pi/3\sqrt{3}a_0 + n\pi/W + k_0$ for integer n. Here k_0 is given by Eq. (4). If the interfaces between strained and unstrained regions are along the y-direction transverse mode number n will be conserved. Hence, $\mathcal{T} = \sum_n \mathcal{T}_n$ and the problem reduces to solving the 1D Dirac equation

$$\left[-i\sqrt{\Sigma_x(x)}\partial_x\sqrt{\Sigma_x(x)} + \Sigma_y q_n + v(x) \right]\psi_n(x) = \mathcal{E}_n\psi_n(x). \tag{7}$$

Here $v(x) = V(x)/\hbar v_F$ is the effective potential in the ribbon and $\mathcal{E}_n = E_n/(\hbar v_F)$.

To calculate $\mathcal{T}$ Eq. (7) should be solved in the regions I, II and III [see Fig. 1(b)] and the solutions matched at the interfaces (see also Ref. 27). In a region of constant v and ϵ, the solution with energy $\mathcal{E}$ in band n is

$$\psi_n(x) = A_n e^{ikx} \begin{pmatrix} 1 \\ e^{i\theta_n(k)} \end{pmatrix} + B_n e^{-ikx} \begin{pmatrix} 1 \\ -e^{-i\theta_n(k)} \end{pmatrix}. \tag{8}$$

where $\exp[i\theta_n(k)] = \frac{k + iq_n}{\mathcal{E} - v}$ and $k = +\sqrt{(\mathcal{E} - v)^2 - q_n^2}$.

The matching of wavefunctions between regions is determined by current conservation [28]. The current-operator corresponding to the Hamiltonian in Eq. (7) is
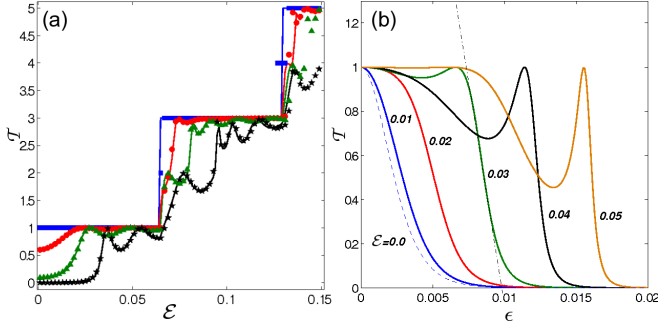
FIG. 2: (Color online) (a) Transmission probability $\mathcal{T}$ through the metallic armchair ribbon ($W = 17$ nm, $L = 28$ nm) [see Fig. 1(b)] as function of $\mathcal{E}$ and ϵ. The solid lines follow from the long wavelength approximation [Eq. (9)] for the strains $\epsilon = 0.0\%$ (blue squares), 0.2% (red circles), 0.5% (green triangles), 1.0% (black stars). The discrete symbols were obtained using numerical tightbinding calculations. (b) Transmission probability $\mathcal{T}$ as function of strain ϵ for energies $\mathcal{E} = 0.0, 0.01, 0.02, 0.03, 0.04$ and 0.05. The slope of the dash-dotted line determines the sensitivity of the working point around $\epsilon = 1.0\%$.

$\hat{J}_x = 2v_F\Sigma_x\sigma_x$. Consequently, at the interface between regions I and II $\sqrt{\Sigma_x^I}\psi_n^I = \sqrt{\Sigma_x^{II}}\psi_n^{II}$. However, the factors $\sqrt{\Sigma_x}$ cancel in the final expression for $\mathcal{T}_n$

$$\mathcal{T}_n(E) = \left(1 + \sin^2\phi_n \left[\frac{\sin\theta_{nI} - \sin\theta_{nII}}{\cos\theta_{nI}\cos\theta_{nII}}\right]^2\right)^{-1}. \quad (9)$$

Here $\phi_n \equiv k_{II}L$ while $\theta_{n(I,II)}$ are the propagation angles for electrons in regions I and II.

In Fig. 2 (a), $\mathcal{T}$ is shown for strains $\epsilon = 0.0 - 1.0\%$ as the solid lines. The discrete symbols, were obtained numerically using the tightbinding Hamiltonian in Eq. (1) and the relation $\mathcal{T} = \text{Tr}[\Gamma_L G_C^r \Gamma_R G_c^a]$. Here $G_C^{r,(a)}$ are the retarded (advanced) Green's functions for the ribbon and $\Gamma_{L,R}$ are self energies accounting for semi-infinite graphene leads. Also, in the numerical calculation, no linearization in strain has been made. As can be seen, for the lowest plateau, a transport gap opens up with increasing strain.

From Eq. (9), the sensitivity of the conductance $G \propto \mathcal{T}$ to ribbon displacements w can be obtained. For the lowest transverse mode $q = 0$ and for $v_{I,II} = 0$ one finds

$$T_0(\mathcal{E}) = \frac{\mathcal{E}^2 - k_0^2}{\mathcal{E}^2 - k_0^2\cos^2 L\sqrt{\mathcal{E}^2 - k_0^2}}. \quad (10)$$

This dependence of $\mathcal{T}$ on ϵ is shown in Fig. 2(b). Different curves correspond to different back-gate bias points, i.e. different values of $\mathcal{E} = 0.0, 0.01, \ldots$. From this figure it is clear how for a given strain, one may chose a working point $\mathcal{E}_0$ (by gating the structure) such that the slope of the $\mathcal{T}(\epsilon)$-curve is maximal. This maximal slope, $|\partial\mathcal{T}/\partial\epsilon|_{\max}$ then defines the sensitivity.
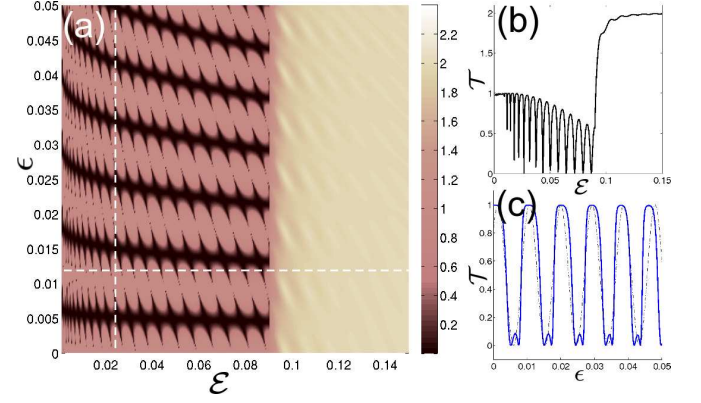

FIG. 3: (Color online) (a) Transmission $\mathcal{T}$ as function of energy $\mathcal{E}$ and strain ϵ through the interferometer shown in Fig. 1(c). Broad dark bands correspond to destructive interference, whereas broad bright bands to unit transmission. The figure was generated using the tightbinding Hamiltonian and recursive lattice Green's function on a system of width $W = 2 \times 7.5$ nm, $L = 24$ nm, and a 'gap' between the ribbons of 0.5 nm. (b) $\mathcal{T}$ as function of $\mathcal{E}$ taken along the horizontal dashed line in panel a. (c) $\mathcal{T}$ as function of ϵ taken along the vertical dashed line in panel (a). The thick solid line is the result of numerical calculation whereas the thin dashed line corresponds to the expression $\sin\phi = \sin[1.8\epsilon(L/a_0)]$.

The smallest sensitivity obtains for the working point at $\mathcal{E} = 0$ [dashed line in Fig. 2(b)]. A lower bound for the sensitivity can be found by setting $\mathcal{E} = 0$ in Eq. (10) and solving for the maximum magnitude of the slope. This gives $|\partial\mathcal{T}/\partial\epsilon|_{\max} \approx \frac{8}{3\sqrt{3}}(L/a_0)$. Hence, for a deflection of magnitude w, the relative change in conductance is $\delta G/G = \delta\mathcal{T}/\mathcal{T} \sim w^2/(La_0)$.

This result is valid for a metallic armchair ribbon where all edges are perfect and impurities absent. For transport restricted to the lowest transverse subband long range impurity scatterers will not affect the transport [29]. However, short range potentials will have effect. For armchair graphene nanoribbons both theory [30], and subsequent experiments [31] suggest that at low temperature, edge disorder induce localization. In this case, transport at low energies is goverend by variable range hopping and strongly supressed. Hence, schemes relying on a single armchair ribbon require nearly perfect edges.

Zig-zag nanoribbons are less sensitive to edge disorder. However, applying strain will not lead to a transport gap. Instead, to obtain a sensitivity of $w^2/(La_0)$ an interferometer with the suspended ribbon making up one of the arms [see Fig. 1(c)] can be used. In graphene ring-geometries Aharanov-Bohm oscillations have been observed at low temperatures [32]. Here, no external B-field is required. Instead, the effective gauge field due to the strain in the suspended arm is exploited.

The idea is again to use the lowest quantized conductance plateau. For zig-zag nanoribbons this is formed from current carried by the edge states. Hence, consider
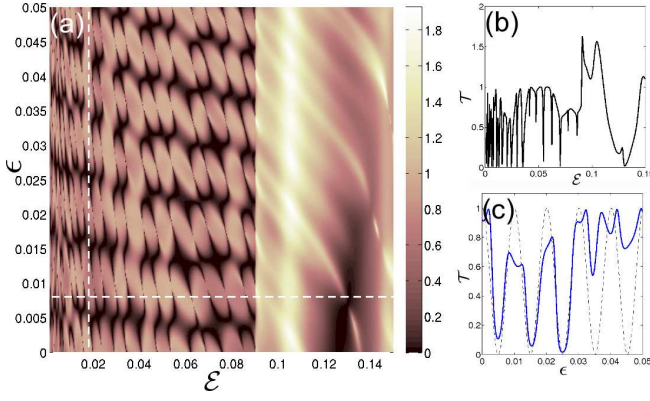
FIG. 4: (Color online) (a) Transmission probability $\mathcal{T}$ as function of energy $\mathcal{E}$ and strain ϵ through the same structure as in Fig. 3, but with added edge disorder (probability to remove edge atoms 30%). (b) $\mathcal{T}$ as function of $\mathcal{E}$ taken along the horizontal dashed line in panel a. (c) $\mathcal{T}$ as function of ϵ taken along the vertical dashed line in panel (a). The thick solid line is the result of numerical calculation whereas the thin dashed line corresponds to the expression $\sin\phi = \sin[1.8\epsilon(L/a_0)]$.

an edge-state coming from the unstrained region I, which split into the two arms IIa and IIb [see Fig. 1 (c)]. The state propagating in the strained arm (IIb) will aquire an extra phase $\phi = k_0 L = 1.8\epsilon(L/a_0)$ [see Eq. (6)], and consequently one expects interference to modulate the conductance with a factor $\propto \sin(\phi)$.

In Fig. 3(a) the result of numerically calculating $\mathcal{T}$ (using the tight-binding Hamiltonian) from region I to region III as function of energy $\mathcal{E}$ and strain ϵ is shown. Bright regions correspond to $\mathcal{T} = 1$ and dark regions to $\mathcal{T} = 0$. These broad dark regions arise due to destructive interference. The fine structure is the result of backscattering at the interfaces where the ribbon split (inter-valley scattering). This is also visible in Fig. 3 (b) where the transmission for a specific strain $\epsilon = 1.2\%$ is shown as function of $\mathcal{E}$.

In Fig. 3(c) $\mathcal{T}$ is shown for a fixed $\mathcal{E}$ as function of strain (thick solid line). The period of the conductance oscillations agree well with the plotted function $1 + \sin\phi$ (thin black line). Hence, approximating $\mathcal{T} \approx 1 + \sin\phi$ yields, as was the case for the armchair ribbon, a sensitivity to deflections of $\delta\mathcal{T}/\mathcal{T} \sim (w^2/La_0)$.

The effect of edge disorder on the interference pattern is shown in Fig. 4(a). Here, disorder has been accounted for by removing the outermost atoms with probability $p = 0.3$ at random along each of the four zig-zag edges of the interferometer. Note that although $\mathcal{T}$ as function of $\mathcal{E}$ [panel (b)] is highly irregular, $\mathcal{T}$ as function of strain [Fig. 4 (c)] show clear conductance modulations. Furthermore, comparing the solid line and the dashed line in Fig. 4 (c), it is clear that the the expression $\sin\phi = \sin[1.8\epsilon(L/a_0)]$ is still valid.

In conclusion, by exploiting the possibility to directly integrate coherent electron transport with graphene nanoribbon NEMS, the conductance through the structure can be made to depend on the mechanical deflection w as $\delta G/G \sim (w^2)/(La_0)$. This is due to the strain induced shift of the Fermi-points (synthetic gauge field). It is this shift which causes the length scale $a_0 \sim \lambda_F \sim 1/k_F$ to enter the expression for δG.

[1] J. S. Bunch, *et al.*, Science **315**, 490 (2007).
[2] D. Garcia-Sanchez, *et al.*, Nano Lett. **8**, 1399 (2008).
[3] J. T. Robinson, *et al.*, Nano Lett., **8**, 3441 (2008).
[4] J. S. Bunch, *et al.*, Nano Lett., **8**, 2458 (2008).
[5] C. Chen *et al.*, Nat. Nanotechn. **4**, 861-867 (2009).
[6] V. Singh, *et al.*, Nanotechn. **21**, 165204 (2010).
[7] C. Berger, *et al.*, Science, **312**, 1191 (2006).
[8] H. B.Heersche, *et al.*, Nature **446**, 56 (2007).
[9] M. Huefner, *et al.*, New J. Phys. **12**, 043054 (2010).
[10] K. I. Bolotin *et al.*, Sol. State. Comm. **146**, 351 (2008).
[11] X. Du, I. Skachko, A. Barker, and E. Y. Andrei, Nat. Nanotechn. **3**, 491 (2008).
[12] S. Adam and S. Das Sarma, Solid Stat. Comm. **146**, 356 (2008).
[13] M. Medvedyeva, and Ya. M. Blanter, arXiv:1006.5010 (2010).
[14] J. Atalaya, A. Isacsson, and J. M. Kinaret, Nano. Lett. **8** (2008).
[15] A. H. Castro Neto, *et al.*, Rev. Mod. Phys. **81**, 109 (2009).
[16] Y. Lee,et al., Nano Lett. **10**, 490 (2010).
[17] M. M. Fogler, F. Guinea, and M. I. Katsnelson, Phys. Rev. Lett. **101**, 226804 (2008).
[18] V. M. Pereira, and A. H. Castro Neto, Phys. Rev. Lett. **103**, 046801 (2009).
[19] E. Prada *et al.*, Phys. Rev. B **81**, 161402(R) (2010).
[20] F. von Oppen, F. Guinea, and E. Mariani, Phys. Rev. B **80**, 075420 (2009).
[21] C. L. Kane, and E. J. Mele, Phys. Rev. Lett. **78**, 1932 (1997).
[22] P. E. Lammert and V. H. Crespi, Phys. Rev. B **61**, 7308 (2000).
[23] L. Yang, and J. Han, Phys. Rev. Lett. **85**, 154 (2000).
[24] A. Kleiner, and S. Eggert, Phys. Rev B. **63**, 073408 (2001).
[25] L. Sun, *et al.*, J. Chem. Phys. **129**, 074704 (2008).
[26] R. M. Ribeiro, *et al.*, New J. Phys. **11**, 115002 (2009).
[27] N. M. R. Peres, Rev. Mod. Phys. **82** (2010).
[28] A. V. Kolesnikov and A. P. Silin, Zh. Eksp. Teor. Fiz. **109** 2125 (1996) [JETP, **82** (6), 1146 (1996)].
[29] M. Yamamoto, Y. Takane, and K. Wakabayashi, Phys. Rev. B **79** 125421 (2009).
[30] I. Martin and Ya. M. Blanter, Phys. Rev. B **79**, 235132 (2009).
[31] M. Y. Han, J. C. Brant, and P. Kim, Phys. Rev. Lett. **104**, 056801 (2010).
[32] S. Russo, *et al.*, Phys. Rev. B **77**, 085413 (2008).